

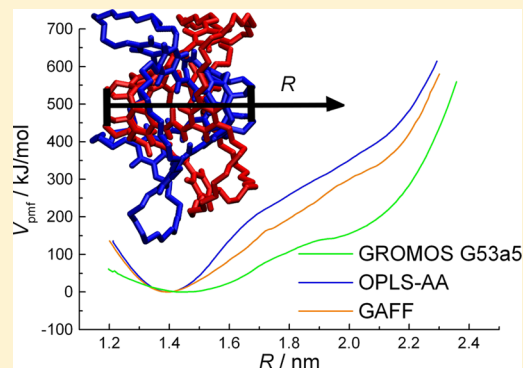
Performance of Different Force Fields in Force Probe Simulations

Thomas Schlesier* and Gregor Diezemann

Institut für Physikalische Chemie, Universität Mainz, Duesbergweg 10-14, 55128 Mainz, Germany

S Supporting Information

ABSTRACT: We present detailed force probe molecular dynamic simulations of mechanically interlocked dimeric calix[4]arene–catenanes, comparing the results obtained using three different commonly used force fields (GROMOS G53a5, OPLS-AA, and AMBER GAFF). The model system is well characterized as a two-state system consisting of a closed compact and an elongated structure. Both states are stabilized by a different hydrogen-bond network, and complete separation of the dimer is prevented by the mechanical lock of the entangled aliphatic loops. The system shows fully reversible rebinding meaning that after bond rupture the system rejoins when the external force is relaxed. We present a detailed study of quantities determined in simulations using a force ramp, like the rupture force and rejoin force distributions. Additionally, we analyze the dynamics of the hydrogen-bond network. We find that the results obtained from using the different force fields qualitatively agree in the sense that always the fully reversible behavior is found. The details, like the mean rupture forces, however, do depend on the particular force field. Some of the differences observed can be traced back to differences in the strength of the hydrogen-bond networks.



■ INTRODUCTION

Molecular dynamic (MD) simulations are a powerful tool for studying the structural and dynamical properties of complex systems. Ideally, one would like to perform *ab initio* MD (AIMD) simulations,¹ which rely on a quantum mechanical computation of the force field. These have the advantage that no *a priori* knowledge about the system investigated is required. Unfortunately, due to the high computational cost of the quantum mechanical methods, AIMD only allows simulations of rather small systems on short time scales. Today, larger systems like solvated biomolecules can be routinely simulated on time scales up to milliseconds using classical MD simulations. Here, the interactions between the particles are approximated by an empirical potential, the force field.^{2,3} For the parametrization of force fields one tries to reproduce properties which are either calculated by quantum mechanical methods^{4–6} or which are accessible experimentally.^{4,7,8} Due to the various parametrization techniques, many different force fields exist.

Quite generally, the accuracy of force fields can be estimated to be about 1–3 kcal/mol for interaction energies.⁹ Since hydrogen bonds in solvated biomolecules have binding energies about 0.5–2 kcal/mol,¹⁰ it is obvious that the results of MD simulations may depend on the force field chosen. For instance, some force fields predict the fast denaturation of RNA and DNA systems which are stable using other force fields.^{11,12} For protein systems, differences are found mainly in the description of the secondary structure. Some force fields facilitate certain secondary structure motifs such as the α -helix or the β -sheet.^{13–16} This has the further implication that the folding pathway (when there is more than one domain which can

unfold) of small proteins is dependent on the choice of the force field, even if the force fields give the correct description of the native structure and the overall folding rate.¹⁷

For the study of systems which fold on time scales longer than microseconds, brute force simulations are not feasible and one needs to use other methods. One approach is to drive the system out of equilibrium by applying an external mechanical force similar to what is realized experimentally in dynamic force spectroscopy.¹⁸ These so-called force probe or steered MD simulations were used for studying folding pathways of proteins^{19,20} and the unbinding of ligands from proteins.²¹

As mentioned above, the performance of various force fields has been investigated for a variety of systems using conventional MD simulations. It is the purpose of the present work to provide such a study for force probe MD simulations. As in such simulations the system is mechanically driven out of equilibrium, this study provides a distinct test of the performance of various force fields. We study and compare the performance of three popular force fields (GROMOS G53a5,⁸ OPLS-AA,^{4,22} and AMBER GAFF⁶) in force probe simulations of a calix[4]arene–catenane dimer system.^{23,24} This system has been investigated before using experiments²⁵ and MD simulations.²⁶ The main feature of the system is a rather simple reaction pathway from a compact to an elongated structure. Since the monomers are interlocked by alkane loops, the dimer cannot completely separate after a rupture event. This allows for reversible transitions between both structures.

Received: November 23, 2012

Revised: January 11, 2013

Published: January 11, 2013

Thus, the performance of the force fields can be investigated for different well-defined nonequilibrium situations. Due to the fact that the transition events are stochastic processes, it is not sufficient to analyze a single trajectory but one needs to determine the distributions of relevant parameters obtained from a large number of simulations. The moderate system size of the calix[4]arene–catenane dimer allows the computation of the required quantities in a reasonable amount of time.

The paper is organized as follows. In the next section we briefly recall the properties of the model system and then present the computational details. Before we show the results of the force probe simulations, we will briefly discuss the structures of the compact and elongated configurations of the system. Finally, we present calculations of the potential of mean force along the reaction coordinate. The paper closes with some conclusions.

■ CALIX[4]ARENE–CATENANES

Calix[*n*]arenes are cuplike structures formed by *n* benzene molecules which are connected via alkyl groups in a ringlike fashion.²⁷ Substituted calix[*n*]arenes are important in the field of host–guest chemistry, since the cage formed by the calix[*n*]arene can enclose various guest molecules,^{28,29} for instance allowing the synthesis of selective sensors.³⁰ The calix[4]arene used in this work is substituted with urea groups at the wide upper rim.^{23,24} In the dimer these urea groups are arranged in a ringlike fashion allowing the formation of a hydrogen-bond network (green in Figure 1) with a maximum

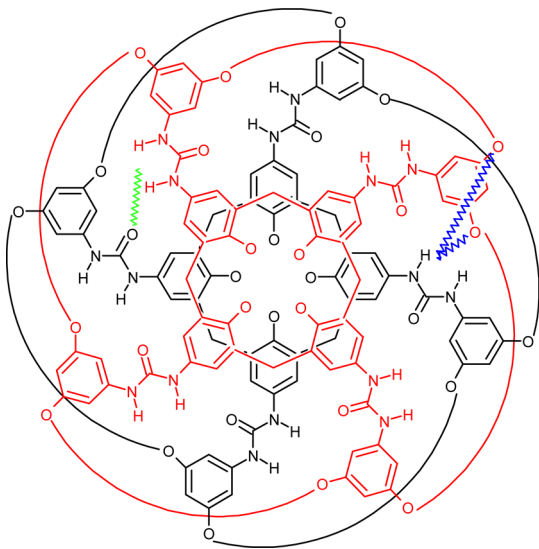


Figure 1. Sketch of the (tetraloop) calix[4]arene–catenane dimer. Each alkane loop consists of 14 CH₂ units. In green (left) the hydrogen bonds between the urea groups (UU-bonds) and in blue (right) the bonds between the urea groups and ether oxygens (UE-bonds) are indicated by the wavy lines. The methoxy groups at the narrow rim in the middle of the figure are abbreviated by “O”.

of 16 bonds. In the following, these bonds will be denoted as UU-bonds. Applying an external force leads to the opening of the UU-bond network and to an elongation of the dimer system. The aliphatic loops of the catenane structure act as a mechanical lock in the dimer system and prevent the complete separation of the monomers, thus facilitating possible rebinding of the two monomers. This way, the catenane structure makes it possible to switch between two different configurations. This

is the reason why interlocked structures like catenanes have attracted attention as possible molecular switches.³¹

In earlier work,^{25,26} it was shown that the extent of the elongation depends on the length of the alkane loops. In the elongated configuration a new set of hydrogen bonds forms. These bonds originate from the interaction of the urea groups of one molecule and the ether oxygens which connect the other monomer to the alkane loops (UE-bonds; blue in Figure 1). Due to sterical reasons, only hydrogen bonds between one ether oxygen and one urea group can form, resulting in a maximum of 16 UE-bonds. In the case of a dimer system with four short alkane loops (14 CH₂ units) per molecule, no further separation of the two molecules is possible. In a system with two longer loops (21 CH₂ units) the UE-bond network can also open and a further separation of the two calixarene cups takes place.^{25,26}

If after stretching the system the force is reduced, a rejoining of the monomers and a re-formation of the UU-bond network is observed. We call this slow reduction of the applied force a relax mode to distinguish it from the pull mode in which the monomers are separated from each other. Experimentally, reversible transitions between the structures involved are observed in both systems investigated. In the simulations only the system with the four short loops shows reversible behavior that is accompanied by a hysteresis.²⁶ For the present work, we chose to investigate this system, because it allows us to investigate the performance of the different force fields under well-defined mechanically induced nonequilibrium conditions. As in the experiments, mesitylene was used as a solvent in all simulations.^{25,26}

■ COMPUTATIONAL DETAILS

All simulations were performed using the GROMACS 4.0.7³² program package employing the three force fields (GROMOS G53a5,⁸ OPLS-AA,^{4,22} and AMBER GAFF⁶). In a first step the topologies for the calix[4]arene–catenane and mesitylene molecules were generated. For the generation process with the GROMOS G53a5 force field the Dundee β -PRODRG2 Server³³ was used and the charges were corrected manually afterward.²⁶ The topologies for the OPLS-AA force field were generated by hand. For the AMBER GAFF topologies first the RESP charges^{34,35} of the molecules were calculated using the REDS Server.³⁶ The geometry optimizations and RESP charge calculations were performed with the Gaussian09 program package³⁷ using the Hartree–Fock method³⁸ with a 6-31G* basis set.³⁹ Afterward the topologies were generated with Antechamber from Amber11⁴⁰ and then converted to a GROMACS format. The parameters for all three force fields are collected in the Supporting Information.

All calculations were performed using periodic boundary conditions. According to the parametrization scheme of the force fields, we applied a short ranged cutoff of 1.4 nm in the case of the GROMOS and the OPLS force field and a cutoff of 1.0 nm for the GAFF force field. Long-range Coulomb interactions were treated with the PME summation method,⁴¹ and for the van der Waals interactions a dispersion correction⁴² was applied. All bond lengths were constrained to their equilibrium value using the LINCS algorithm⁴³ allowing a time step of 2 fs. The effect of the externally applied forces has only a negligible effect on the bonded interactions because they always are much smaller than the intramolecular forces. The neighbor list was updated every 5 steps (10 fs). The simulation box was

rectangular (about 5.4 nm × 4.4 nm × 4.4 nm) and included one calix[4]arene dimer and around 440 mesitylene molecules.

In the actual simulations the following protocol was used. In a first step the structures of the isolated calix[4]arene dimer and a mesitylene molecule were optimized. After solvating the calix[4]arene dimer, a second geometry optimization for the total system was performed. The solvated system was equilibrated at 300 K for 500 ps using a velocity recycling thermostat⁴⁴ (time constant 0.1 ps). After this the system was coupled to a barostat with a pressure of 1 bar for 1 ns using a Parrinello–Rahman barostat⁴⁵ with a time constant of 2.0 ps and a compressibility of $8.26 \times 10^{-5} \text{ bar}^{-1}$.⁴⁶ After the equilibration process the production simulations were performed with the same parameters for the thermostat and the barostat.

For all the force probe simulations the center of mass of the four carbon atoms of the methoxy groups at the narrow rim of one calix[4]arene were fixed (reference group) and we applied a time-dependent harmonic pulling potential to the center of mass of the carbon atoms of the methoxy groups of the other molecule (pulled group); see Figure 2. The distance between

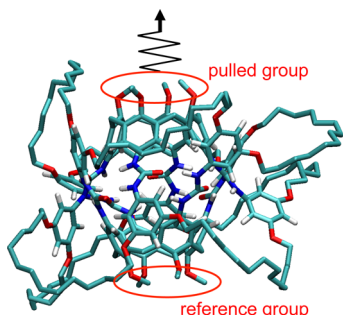


Figure 2. Stick model of the calix[4]arene–catenane dimer (only polar hydrogens are shown) and sketch of the pulling device showing the reference and the pulled group.

these two groups is the end-to-end distance R . The force F acting on the pulled group is given by

$$F = k(vt - z) \quad (1)$$

where k is the force constant of the pulling spring, v the pulling velocity, and z the displacement of the pulled group from its initial position. The pulling spring moves along the vector connecting the reference group and the pulled group. All simulations were performed with a force constant of $k = 830.5 \text{ pN/nm}$ and pulling velocities of $v = v_{\text{fast}} = 1 \text{ m/s}$ and $v = v_{\text{slow}} = 0.1 \text{ m/s}$, which are typical values for MD simulations.⁴⁷ For v_{fast} we performed 100 simulations and for v_{slow} 50 simulations each consisting of a pull-mode and a relax-mode simulation. In order to observe all transition events the system was simulated for 3 ns for v_{fast} and 25 ns for v_{slow} in the case of the GROMOS force field. For the OPLS and GAFF force fields we used 3.5 and 30 ns, respectively. In the relax mode the same parameters as in the pull-mode simulations were used with the difference that the pulling direction was reversed and as a starting structure the last configuration of the respective pull-mode simulation was used.

In order to investigate the hydrogen-bond network dynamics, we assumed a closed hydrogen bond if the distance between the hydrogen donor and acceptor is smaller than 0.35 nm and if the angle formed by the three atoms is less than 30° . Earlier studies²⁶ showed that the results of the analysis are

independent of the particular choice of these geometric parameters over a rather wide range (distances between 0.3 and 0.4 nm and maximum angles in the range of $25\text{--}40^\circ$).

■ STATIC PROPERTIES

For each force field we performed two kinds of simulations to characterize the closed and open state. The first one was an equilibrium simulation without an external force. From this simulation one can extract information about the closed state. The other type of simulation was performed to investigate the open state of the system. This state is defined by the configurations which result from the force probe simulations after the breaking of the UU-bonds, the elongation of the system and the formation of the UE-bonds. Since this state is only stable under an external load, we had to apply an external force along R to stabilize these configurations.

Closed State. The closed state is the equilibrium state of the system at a temperature of 300 K. To compare the results obtained for different force fields and to characterize the structures of the closed state we performed NPT simulations for 20 ns. The root-mean-square displacement (rmsd) for all three force fields is similar. The calixarene dimers show two main structural features, as the monomers consist of a compact cuplike arrangement and the rather floppy alkane chains. As expected from the rigidity of the cups, the dominant contribution to the rmsd stems from the alkane chains.

In order to compare the conformational flexibility of the alkane chains, we determined the probability distribution function (PDF) of the distances between the center of mass of the whole dimer (red dot in Figure 3) and the center of each

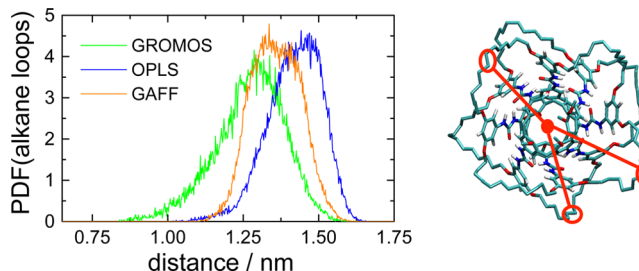


Figure 3. Left: PDF of the alkane chains. Right: Sketch for the PDF distances between the COM of the whole dimer (red dot) and the middle of each alkane chain which is given by the COM of the two innermost carbon atoms (open circles).

alkane chain which is given by the center of mass of the two innermost carbon atoms (open circles in Figure 3). The distribution for the GAFF force field is rather symmetric as opposed to the ones for the other force fields which show some skewness. The width as determined by the second moment, however, is very similar for all three force fields and amounts to about 0.25 nm. Thus, there are no significant differences in the overall flexibility of the aliphatic loops.

Figure 4 shows the PDF of the end-to-end distance R which is an important structural property since it is the reaction coordinate for the force probe simulations (cf. Figure 2). The distributions for the OPLS and GAFF force field are more or less identical and the centers of the distributions are located at $R \approx 1.40 \text{ nm}$ in both cases. The distribution for the GROMOS force field is peaked at significantly larger distances (1.46 nm) and is much broader. For the GROMOS force field the width of the distribution is around 0.1 nm, and for the other two force

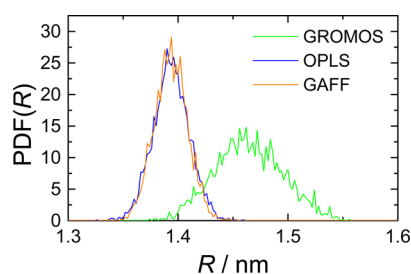


Figure 4. PDF of the distance between the reference group and the pulled group, R .

fields it is roughly 0.04 nm. From this one can conclude that the dimer is more flexible along the reaction coordinate in the case of the GROMOS force field compared to the other two force fields.

To understand the different flexibility along R for the different force fields, it is important to investigate the hydrogen-bond network, since these bonds stabilize the compact structure of the dimer and inhibit the free movement of the molecules. The OPLS and GAFF force fields on average form 15–16 UU-bonds, whereas the GROMOS force field shows only about 10 bonds. The smaller number of hydrogen bonds results in a weaker binding between the two cups giving rise to a larger end-to-end distance and a broader distribution due to a larger flexibility of the system. As will be detailed below, the weaker binding of the dimer for the GROMOS force field has also a huge impact on the rupture force distribution in the pulling simulations.

Open State. As mentioned above, the open state of the dimer system is not an equilibrium state at 300 K. In order to investigate it one has to apply an external force to stabilize its configurations. For all three force fields, we used a force of 1000 pN. The starting structures for the simulations were obtained from relax-mode simulations with v_{slow} . The reason for using the relax-mode simulation for the generation of a starting structure instead of a pull-mode simulation is that one can exploit the hysteresis to obtain an open configuration at a smaller force (see Figure 8 for the transition forces). In each case, we used a configuration from the trajectory in which the applied force was near 1000 pN. The production simulation lasted 25 ns and the last 20 ns were used for analysis purpose. Figure 5 shows the PDFs for the open state.

The differences between the force fields in the PDFs for the alkane loops of the open state are smaller compared to the ones of the closed state. The centers of the distributions are shifted to slightly smaller distances and the widths are smaller. Both observations can be attributed to the fact that in the open state

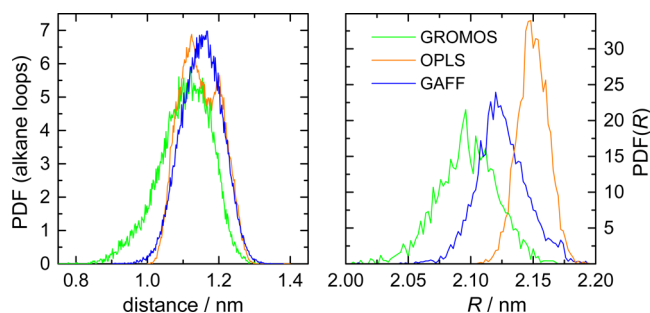


Figure 5. PDF of the alkane loops (left, for definition see Figure 3) and the PDF of R (right) for the open state.

the whole dimer is stretched. The stretched loops have less configurational freedom than the loops in the closed state. The PDF for R shows that the dimer is significantly stretched to 2.1 and 2.12 nm for the GROMOS and OPLS force field and to 2.15 nm for GAFF. Concerning the number of UE-bonds stabilizing the open state, one observes on average 10 bonds for the GROMOS and GAFF force field and 7 for the OPLS force field.

FORCE PROBE SIMULATIONS

The previous section showed that the three force fields behave similarly in equilibrium simulations. In this section we investigate the performance under well-defined nonequilibrium conditions, the application of a time-dependent force. Qualitatively, all three force fields show the same behavior, namely the transition between the closed and the open state. Only the actual number of hydrogen bonds and the forces at which the transitions take place vary. In the following, we will discuss different observables (number of hydrogen bonds, force–extension (FE) curves, etc.) of a single trajectory. For the GROMOS force field, a detailed analysis of force probe simulations can be found in ref 26. After a brief discussion of a sample trajectory, we present a detailed comparison of the three force fields. Due to the random nature of the rupture process the dynamics of the previously mentioned observables will differ slightly in each trajectory. In order to not compare single trajectories, we averaged the results over all simulations for each force field and pulling velocity.

Sample Trajectory. The end-to-end distance and the force acting on the system of a sample trajectory are shown in the left panel of Figure 6. On the right panel the number of hydrogen

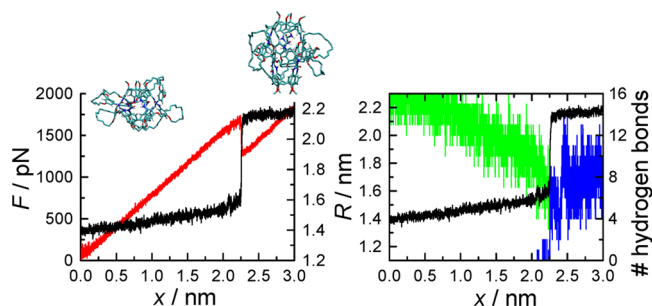


Figure 6. Sample trajectories with $v_{\text{slow}} = 0.1$ m/s. Left: End-to-end distance R (black) and FE curve (red) for the OPLS force field. Additionally shown are typical structures for the closed (left) and for the open (right) state. Right: Number of hydrogen bonds (UU-bonds (green) and UE-bonds (blue); cf. Figure 1) and R (black).

bonds are shown. The simulation employed the OPLS force field and the pulling velocity $v_{\text{slow}} = 0.1$ m/s. In the figure the observables are plotted against the extension $x = vt$. During the pulling the force (red) increases linearly, the end-to-end distance R (black) increases gradually, and a few UU-bonds open (green). At an extension of about 2.25 nm all remaining UU-bonds open abruptly and R increases in a stepwise fashion indicating the formation of the open structure. At the same time, a new set of hydrogen bonds consisting solely of UE-bonds (blue) is developed. After the rupture event the force decreases by a significant amount since the spring relaxes due to the sudden increase in R . The insets show typical structures for the closed and open state.

Figure 7 shows typical FE curves for all three force fields.

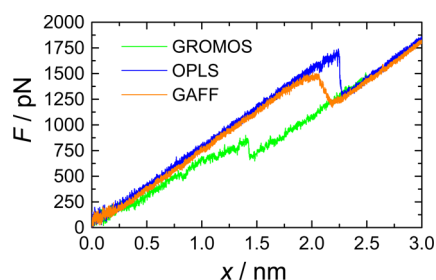


Figure 7. Sample FE curves for the three force fields: GROMOS (green), OPLS (blue), and GAFF (orange).

The smaller slope of the curve before the rupture event in the case of the GROMOS force field originates from the larger flexibility of the dimer in the closed state. One can relate the slope (dF/dx) to an effective force constant; for details, see eq 2 in the section about the Dynamic Strength.

The force corresponding to the extension at which the opening of the dimer occurs is called rupture force. Since the rupture event is a stochastic process, it is meaningless to compare rupture forces of single trajectories. To get a deeper understanding of the mechanism of the rupture process, it is mandatory to perform a large number of simulations and analyze the statistical properties of the results.

Rupture and Rejoin Force Distributions. As already mentioned above, we performed a large number of force probe simulations in both the pull and the relax modes. For each FE curve, we determined the rupture (rejoin) force manually. The resulting distributions are displayed in Figure 8 for the three

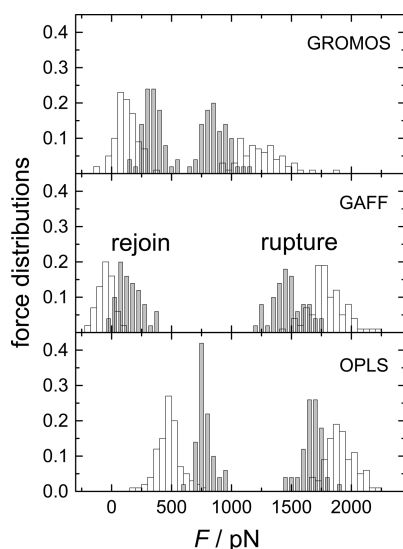


Figure 8. Rupture (right) and rejoin (left) force distributions for $v_{\text{fast}} = 1$ m/s (white) and $v_{\text{slow}} = 0.1$ m/s (gray). The distributions were normalized to the total number of simulations.

force fields. Assuming that the strength of a single hydrogen bond is roughly identical for each force field and that the number of bonds is proportional to the rupture force, one can explain the trend in the rupture forces. The rupture force distributions of the GROMOS force field are shifted to smaller forces compared to the other two force fields, which is in accord with the smaller number of UU-bonds (10 instead of 15–16) in the equilibrium simulation of the closed state. In the case of the OPLS and GAFF force fields for which the number

of observed hydrogen bonds is the same, the differences in the distributions are much smaller. The increase of the rupture force with pulling velocity is in agreement with the simple Bell model which predicts that the rupture force depends logarithmically on the pulling velocity.⁴⁸

The rejoin forces all are significantly smaller than the rupture forces. As expected, the difference between the mean rupture force and the mean rejoin force increases with increasing pulling velocity. Similar to the rupture forces, one can qualitatively relate the rejoin forces to the average number of UE-bonds stabilizing the open state. For the OPLS force field, fewer UE-bonds are observed as for the GROMOS and GAFF force field which is in accord with the larger rejoin forces. This simple argument, however, cannot explain the differences observed when comparing the GROMOS and the GAFF force field, because for these very similar numbers of UE-bonds are observed.

Dynamic Observables. In the following, the mean values of dynamic observables, namely the dynamic strength and the end-to-end distance, will be discussed. Averages were performed using all simulations for a given force field and pulling velocity.

Dynamic Strength. The dynamic strength $\langle F \rangle$ is given by the averaged FE curves^{49–51} and is a bulk property. The determination of this quantity can be quite meaningful when two-state systems near equilibrium are considered. In this situation, fluctuations may hamper or even completely prevent the determination of the individual transition events⁵² and the rupture force distribution. The dynamic strength has the additional advantage that one can extract elastic properties of the system.⁵¹ Furthermore, it is an useful observable in the description of adhesion clusters, where it is not possible to observe the rupture of individual bonds.

We calculated the dynamic strength $\langle F \rangle$ by averaging all FE curves (50 for $v_{\text{slow}} = 0.1$ m/s, 100 for $v_{\text{fast}} = 1$ m/s) and present the results in Figure 9. In contrast to a single FE curve, the dynamic strength shows no stepwise reduction of the force. The reason for this is the stochastic nature of the rupture events. Due to the different rupture forces, the events occur at different extensions, and the stepwise drop in the force gets

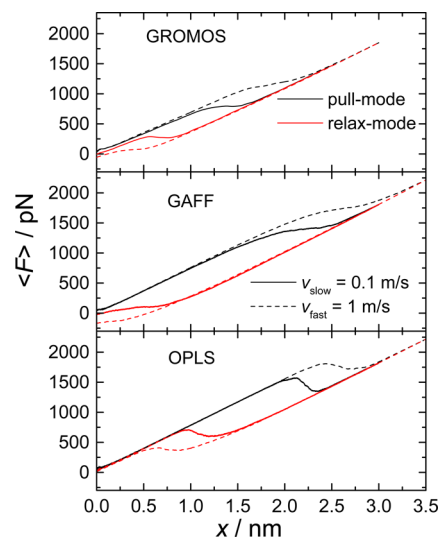


Figure 9. Dynamic strength for all three force fields. The pulling simulations are shown in black and the relax-mode simulations in red. Full lines indicate $v_{\text{slow}} = 0.1$ m/s and the dashed lines $v_{\text{fast}} = 1$ m/s.

averaged out. This effect is ν -dependent since the width of the rupture force distributions depends on the pulling velocity. The ν -dependent hysteresis as seen in the transition force distributions is also observed in the dynamic strength.

In some relax-mode simulations, especially for ν_{fast} in the case of the GAFF force field, one observes negative values for $\langle F \rangle$. The reason for this is that in some simulations the system does not “find” the closed state. This topic will be discussed in the next section.

It is possible to determine elastic properties from the dynamic strength. The slope of $\langle F \rangle_\omega$ where α determines the state (closed/open) of the system, in a Gaussian approximation⁵¹ is given by an effective force constant

$$k_{\text{eff}}^\alpha = \frac{k k_{\text{mol}}^\alpha}{k + k_{\text{mol}}^\alpha} \quad (2)$$

where k denotes the force constant of the cantilever and k_{mol}^α is the curvature of the free energy minimum in a harmonic approximation, which will be denoted as the molecular force constant in the following. The values obtained for the molecular force constant are given in Table 1, and we estimate

Table 1. Molecular Force Constants of the Calix[4]arene Dimer for Both the Closed (c) and Open (o) Structure

force field	$k_{\text{mol}}^{\text{c}}/(\text{pN/nm})$	$k_{\text{mol}}^{\text{o}}/(\text{pN/nm})$
GROMOS	3140	7050
GAFF	6960	14670
OPLS	10960	10570

the error to be about 20–30%. The values of the molecular force constant are in accord with the width of the PDF(R) for the individual states. In the case of the closed state, one observes a larger width for the GROMOS force field compared to the other two force fields. This corresponds to a larger flexibility of the system along the reaction coordinate, which is in accord with the smaller molecular force constant. In the open state one notices for the GROMOS and GAFF force field an increase in k_{mol} , which is in accord with the observed narrowing of the PDF(R) of the open state compared to the closed state (cf. Figures 3 and 5).

End-to-End Distance. An important structural parameter that changes during a pulling simulation and sensitively depends on the details of the force field is the end-to-end distance R . An example of its evolution during a pulling simulation has been shown in Figure 6. In Figure 10 we present the values averaged over all force probe simulations.

For all three force fields, $\langle R \rangle$ starts at around 1.4 nm and converges to a value of 2.2 nm in the limit of strong forces. The ν -dependent hysteresis which is observed in the dynamic strength is also found in $\langle R \rangle$. Similar to the dynamic strength where the sudden drop of F of the individual simulations gets averaged out, one does not observe a step in $\langle R \rangle$ but a sigmoidal shape.

It is obvious that the slopes at small extensions for the OPLS and GAFF force fields are significantly smaller than the slope for the GROMOS force field, which is expected from the smaller molecular force constant in case of the GROMOS force field. A weaker force constant corresponds to a system which is more flexible and thus is more easily stretched.

The reversible behavior of the force fields can be characterized by the difference in $\langle R \rangle$ between the start and the end of the pull-relax circle. One notices that this difference

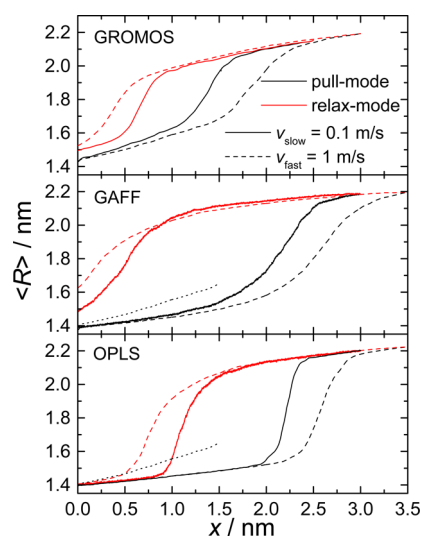


Figure 10. $\langle R \rangle$ for all three force fields. The results of pull-mode simulations are shown in black and those of relax-mode simulations in red. Full lines indicate $\nu_{\text{slow}} = 0.1$ m/s and the dashed lines $\nu_{\text{fast}} = 1$ m/s. The dotted lines represent the slope of the pull-mode simulations for the GROMOS force field.

depends on ν which is a consequence of the nonequilibrium nature of the force probe simulations. In the limit of infinite slow pulling, it is to be expected that no difference is observed. A finite difference implies that not all relax-mode simulations end in a structure which is similar to the starting structure. We denote the gap in $\langle R \rangle$ at zero extension between the pull-mode and relax-mode simulation by $\Delta R = R_{\text{relax}}(x=0) - R_{\text{pull}}(x=0)$. In the case of the OPLS force field, even for ν_{fast} almost no gap is observed. For the GROMOS and especially the GAFF force field ΔR is larger, 0.05 and 0.1 nm respectively. There are two reasons for the observed gap. In some simulations the calixarene dimer simply does not rebound on the simulation time scale. Especially in the case of the GAFF force field employing the fast pulling velocity, only a few simulations show the rebounding to the closed state. In other simulations, a mesitylene molecule diffuses between the two cups while the system is in the open state. The dimer still might rejoin, but due to the trapped mesitylene molecule one observes a slight increase in R .

To estimate the amount of simulations in which the dimer rebounds, we consider only such simulations in which $R_{\text{relax}}(x=0)$ is in the range of values which are found in the equilibrium simulation of the closed state (see PDF(R) and Figure 4). The results are given in Table 2. From Table 2 it is clear that the system in the case of the OPLS force field shows an almost complete reversible behavior. At $x = 0$ most of the relax-mode

Table 2. p_{rejoin} Gives the Fraction of Simulations Which Reach the Closed State as Defined in the Text at the End of the Relax-Mode Simulation

force field	$\nu/\text{m/s}$	p_{rejoin}
GROMOS	0.1	0.88
	1	0.73
GAFF	0.1	0.52
	1	0.07
OPLS	0.1	0.96
	1	0.95

simulations exhibit a value for R which is in the range of the corresponding PDF(R). For the other two force fields, one observes a significant decrease in the rebinding probability if the pulling velocity is increased. In the case of the GROMOS force field we have shown in ref 26 that at $v = 10$ m/s the system turns completely irreversible and one observes no rebinding events. This is a manifestation of the nonequilibrium nature of the force probe MD simulations.

Potential of Mean Force. In addition to the force probe simulations, we also determined the potential of mean force (PMF), which is the free energy surface of the system as a function the reaction coordinate. We used the thermodynamic integration (TI) technique,^{53,54} where one generates several configurations of the system along the reaction coordinate which is the end-to-end distance R in our case. By integrating the forces F_c which are required to constrain the configurations to the individual points of the reaction coordinate, one can obtain the PMF

$$V_{\text{pmf}}(R) = - \int_R^{R_{\text{max}}} \left[F_c(s) + \frac{2k_B T}{s} \right] ds$$

where R_{max} is the maximum distance of R ⁵⁴ and $((2k_B T)/s)$ is a Jacobian factor.

Configurations of the dimer were generated with R between 1.2 and 2.3 nm and a spacing of 0.01 nm by pulling along the reaction coordinate in both directions with a velocity of $\dot{R} = 0.1$ m/s. In the production simulations, R was constrained and F_c was recorded over 3 ns after an equilibration period of 1.2 ns. To be sure that the PMF is not biased by the pulling simulations which were used for the generation of the starting configurations, we determined the PMF three times using configurations which were generated by different pulling simulations. Since the differences were negligible, we show the averaged results in Figure 11 (full lines). Qualitatively, the

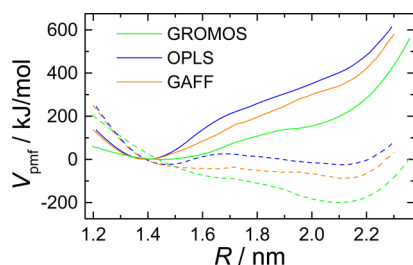


Figure 11. Potential of mean force for all three force fields. Full lines represent the force-free PMF and dashed lines indicate the PMF if the system is subjected to an external force of 1000 pN. The energy is scaled such that $V_{\text{pmf}}(0, R_{\text{eq}}) = V_{\text{pmf}}(F, R_{\text{eq}}) = 0$.

shape of the PMF for the three force fields is similar. In the range of $R = 1.2$ – 1.7 nm, one observes a region in which the PMF is almost harmonic. The global minima at $R = 1.4$ – 1.45 nm correspond to the closed states. Going to larger distances, the energy rises and at around $R = 2.1$ – 2.2 nm the slope strongly increases. At this distance, the open state is located and the increase in the slope is due to the fact that the alkane loops get stretched and lose their flexibility.

For small value of R the PMFs of the OPLS and GAFF force fields are similar which is expected due to the comparable behavior in the pull-mode simulations. For these force fields the curvatures of the global minima are larger than for the GROMOS force field, which is expected by the PDF(R) (cf.

Figure 4) and the molecular force constants (cf. Table 1). In the case of the GROMOS and OPLS force field it is possible to determine k_{mol} by fitting the global minima by a harmonic potential. For the GROMOS force field we find $k_{\text{mol}} = 3990$ pN/nm and for the OPLS force field $k_{\text{mol}} = 14\,950$ pN/nm, which in both cases is larger than the values that are determined from the dynamic strength (cf. Table 1). In case of the GAFF force field the molecular force constant is not determined due to the deviations of the potential from a harmonic shape. The energy difference between the position of the open state ($R \approx 2.1$ nm) and the global minimum is much smaller for the GROMOS force field than for the other two force fields. This is in accord with the smaller rupture force for the former force field.

Applying an external force to the dimer system will result in a change of the PMF. In the simplest model, the force-dependent PMF is given by

$$V_{\text{pmf}}(F, R) = V_{\text{pmf}}(0, R) - RF \quad (3)$$

The results obtained by eq 3 are shown as dashed lines in Figure 11. The change in the PMF by applying a force to the dimer has a different impact for the three force fields. In the case of the GROMOS force field the open state becomes the global minimum and the closed state is hardly visible at 1.6 nm. For the OPLS force field the PMF shows two minima which are separated by a small energy barrier at around 1.68 nm. In case of the GAFF force field the PMF is almost flat. These trends correspond well to the rupture force distributions for the slow pulling velocity. In the case of the GROMOS force field a rupture force which is significantly smaller than the applied force of 1000 pN is observed, and therefore the open state becomes much more favorable. For the OPLS and GAFF force field one does not observe a preference of the open state compared to the closed state. This is in accord with the average rupture force, which is in both cases larger than 1000 pN. For both force fields the two states roughly have the same energy. The most probable value of R for the open state (cf. Figure 5) is in good agreement with the local minimum of the PMF.

The traditional definition of a transition state is the local maximum between the local minima of the two states. The exact position of the transition state in the calixarene dimer system cannot be determined, since no local maximum of the PMF is observed. But one can estimate the transition state from the force-shifted PMF. In the Bell model one assumes that the position of the transition state is not affected by the force probe experiment. In the case of the force-shifted PMF of the OPLS force field (dashed blue line in Figure 11), one observes a local maximum at $R = 1.7$ nm. At this distance the force-free PMF also changes the slope for all three force fields. Thus, one could argue that the position of the transition state is around $R \approx 1.7$ nm.

Hydrogen-Bond Network. As mentioned above, the hydrogen-bond network plays an important role in the characterization of the calixarene-dimer system. To begin with, we investigate the dynamical behavior of the hydrogen bonds. In Figure 12, the average number of H-bonds is shown as a function of the extension x .

The average number of H-bonds shows a broadening of the transition events when compared to a single trajectory (cf. Figure 6), similar to $\langle R \rangle$ and the dynamic strength. For the OPLS and GAFF force field, the maximum number of 16 UU-bonds is found in the closed state, while for the GROMOS force field there are only 8–10 UU-bonds. Concerning the

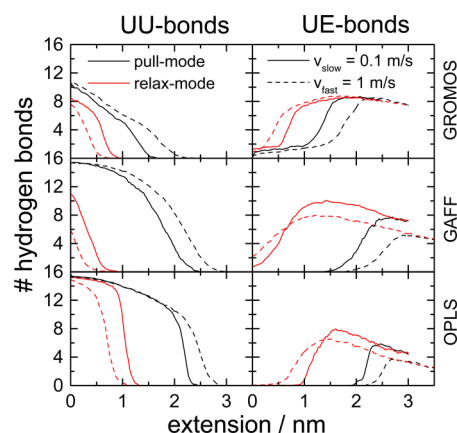


Figure 12. Average number of hydrogen bonds: (left panels) UU-bonds; (right panels) UE-bonds.

open state, one observes on average 8–10 UE-bonds for all three force fields. The general behavior of the hydrogen-bond network in the force probe simulations resembles that of the dynamics of the other observables. For instance, in the case of the OPLS force field the number of H-bonds changes much faster around the transition event as for the other two force fields. For all three force fields one observes fewer UU-bonds at the end of the relax-mode simulation than at the beginning of the pull mode. This effect has the same origin as the gap in $\langle R \rangle$ and the force fields dependence is the same; i.e., for the OPLS force field the number of UU-bonds at the start and end of the pull–relax cycle hardly changes, while for the GAFF force field the largest difference is found. In the case of the OPLS and GAFF force field one observes slightly more UE-bonds in the relax-mode simulations than in the pull mode.

One major difference in the case of the GROMOS force field is that the number of UU-bonds during the pull-mode simulations decreases in an almost linear fashion, whereas for the OPLS and GAFF force fields first a slow decrease which becomes much steeper at larger extensions is observed. The latter nonlinear behavior is also found in kinetic Monte Carlo simulations of adhesion clusters under shared linear load.⁵⁵ The difference in the dynamics of the UU-bonds can be explained by a different strength of the two hydrogen bonds which are formed by one urea group pair. The dynamics of both UU-bonds of one urea group pair for a typical pull-mode simulation are shown in Figure 13. In the case of the OPLS force field both UU-bonds open at the same time, while for the GROMOS force field there is a significant delay between the rupture of the first and the second bond. For the GAFF force field one observes a behavior which is in between these extreme scenarios. The different strength of the UU-bonds in the case of the GROMOS force field explains the smaller average number of UU-bonds compared to the other two force fields and consequently the smaller molecular force constant of the closed state. In the case of the hydrogen-bond network, it is also interesting to investigate the number of bonds as a function of R instead of x . While the latter approach allows to follow the details of the nonequilibrium dynamics, considering the number of H-bonds as a function of R gives information about the relevant structures. There are two ways to obtain a plot of the number of hydrogen bonds from the data. One can determine the number of bonds from the individual configurations that are used to calculate the potential of mean force. This more or less presents a static or equilibrium

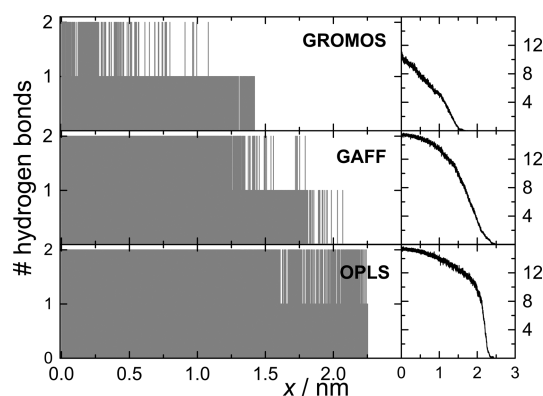


Figure 13. Dynamics of the two UU-bonds for one urea group pair in a typical pull-mode simulation. Each trace shows the number of bonds (zero, one, or two) located at one pair of two neighboring urea groups. On the right, the total number of the UU-bonds for v_{slow} are depicted.

approach, since the system can relax in each configuration to a quasi-equilibrium under the constraint of fixed R . The alternative involves the use of the data from force probe simulations, where one computes R and the number of H-bonds as a function of x . This allows to treat the number of H-bonds as a function of R . Compared to the static approach via PMF calculations, this would be a dynamic or nonequilibrium description of the hydrogen-bond network. We performed this analysis for each individual force probe simulation and afterward we averaged over all pull-mode and relax-mode simulations separately. In the case of the relax-mode simulations, we considered only simulations in which the dimer rejoins since including the other simulations also would introduce a bias toward a smaller number of hydrogen bonds at small extensions x .

Figure 14 shows the data from the equilibrium approach.

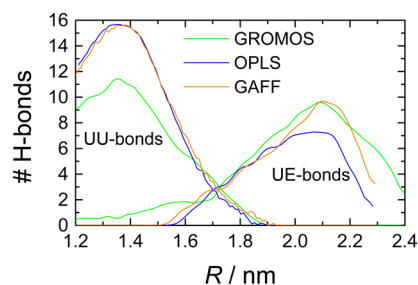


Figure 14. Number of hydrogen bonds vs R determined from the configurations that are used to calculate the PMF. On the left side the UU-bonds are shown and on the right side the UE-bonds.

The closed state is located at around 1.4 nm with about 16 UU-bonds in the case of the OPLS and GAFF force field, while for the GROMOS force field only 11 bonds are found. The trend of number of UU-bonds for the OPLS and GAFF force field is very similar which is in accord with the similarities seen in the dynamic properties. The open state is located at 2.1 nm and 10 UE-bonds are found for the GROMOS and GAFF force fields. In the case of the OPLS force field, fewer (7) UE-bonds are observed, which could explain the different rejoin forces of the OPLS and GAFF force fields. But apart from these minor differences, the curves for all force fields look quite similar.

At around 1.7 nm the curves for the UU- and UE-bonds cross each other and around three bonds of both types are

observed. This distance corresponds to the distance at which the transition point is to be expected from the potential of mean force.

For the nonequilibrium approach only the data from the simulations with the slow pulling velocity are shown in Figure 15. For v_{fast} one observes almost the same results. The data

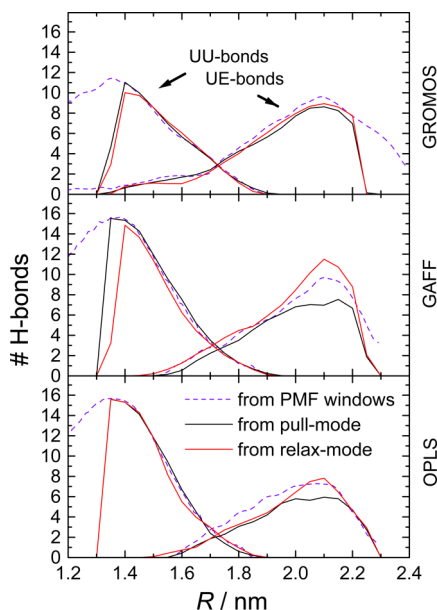


Figure 15. Number of hydrogen bonds vs R determined from the pull-mode (black) and relax-mode (red) simulations for v_{slow} . The results from the configurations of the PMF calculation (Figure 14) are shown as a reference (dashed violet).

from the force probe simulations (black for pull mode and red for relax mode) reproduces the data that is obtained from the PMF calculation (dashed violet) quite well. The main differences are found in the number of the UE-bonds, where the number of bonds observed in the relax-mode simulations is a little bit larger compared to the pull-mode simulations. Concerning the force probe simulations, this effect is also observed in plot versus x ; see Figure 12. Apart from this, the differences between the two approaches are almost negligible, which is remarkable since the approach via the force probe simulations relies on nonequilibrium simulations, while the determination using the configurations from the PMF calculation involves equilibrium simulations under a constraint.

CONCLUSIONS

We presented well-defined nonequilibrium simulations of a calix[4]arene–catenane dimer system. By applying a time-dependent external force, it is possible to transfer the system from the equilibrium closed state to an elongated open state, which is only stable under the influence of an external force. In a simple picture, one can approximate the system by a two-state model, in which both states are well separated.

It is not unexpected that all three force fields qualitatively yield similar results and reproduce the reversibility of the system due to the constraint nature of the calix[4]arene dimer and the well-defined reaction pathway. But the details depend on the force field chosen. The configurations in the equilibrium simulations of both states are similar for all force fields, the most probable R differs by less than 0.1 nm ($\approx 7\%$), and the differences for the open state are even smaller than for the

closed state. In the equilibrium simulations of the closed state, the GROMOS force field differs from the other two force fields by the smaller number of UU-bonds, which affects the rupture force distributions strongly. For the GROMOS force field, much smaller rupture forces, compared to the other two force fields, are observed which is in accord with the smaller number of hydrogen bonds present in the closed state. The performance of the OPLS and GAFF force field in the pull-mode simulations is very similar, which is also expected from the similar rupture force distributions. In the case of the relax-mode simulations, one finds a similar trend concerning the UE-bonds and the mean rejoin forces. For the OPLS force field one observes fewer UE-bonds in the open state and the rejoin forces are significantly larger compared to the other two force fields for which one finds almost the same number of UE-bonds and comparable rejoin forces. The reason that in this case less hydrogen bonds correspond to a larger rejoin force is that fewer hydrogen bonds stabilize the system to a lesser degree which results in an earlier transition.

Concerning the rebinding behavior, one observes differences between all three force fields. In the case of the OPLS force field almost all relax-mode simulations end in the closed state with the maximum number of hydrogen bonds, while for the GAFF force field one observes a much smaller (average) amount of UU-bonds at the end of the relax-mode simulations due to the fact that only in a few simulations the dimer rejoins completely. The different rebinding behavior is not only observed in the number of UU-bonds but also in end-to-end distance R at the end of the relax-mode simulation. Nevertheless, the three force fields show a similar reaction pathway, i.e., number of hydrogen bonds versus R . It is quite remarkable that the static approach (performing equilibrium simulations under the constraint of a fixed R) and the dynamic approach (force probe simulations) yield qualitatively the same results for the reaction pathway. Contrary to the dynamic observables (F , R , and the number of hydrogen bonds) for which one observes a hysteresis in the force probe simulations, the reactions pathway is rather unaffected by the pulling direction.

The dynamics of the force probe simulations depend to a different degree on the pulling velocity. Generally, larger pulling velocities drive the system stronger out of equilibrium and render the system more irreversible but the magnitude of this effect depends on the force field chosen.

In summary, the three force fields show similar results on a qualitative level and reproduce the reversibility of the system. In the case of static observables, like the reaction pathway, the force fields give much more similar results compared to the dynamic observables which are measured during the force probe simulations. Furthermore, it is remarkable that the results for the reaction pathway depend only slightly on the method (static or dynamic) or on the pulling direction (pull- or relax-mode in the case of the dynamic approach) while for the dynamic observables a hysteresis is observed.

Although our results look promising, it is to be expected that, in more complex systems, which do not exhibit a simple reaction pathway, the differences between different force fields might be larger. More importantly, if there is more than one reaction pathway the probability of choosing a particular pathway may depend on the force field. Our study shows that the situation regarding the reliability of the force fields used in MD simulations is not complicated additionally if the system is exposed to an external force and driven out of equilibrium. This

means that we can safely assume a computational accuracy that is comparable to the one of equilibrium simulations.

■ ASSOCIATED CONTENT

■ Supporting Information

The force field parameters used in the MD simulations are tabulated. This material is available free of charge via the Internet at <http://pubs.acs.org>.

■ AUTHOR INFORMATION

Corresponding Author

*E-mail: schlesi@uni-mainz.de.

Notes

The authors declare no competing financial interest.

■ ACKNOWLEDGMENTS

Financial support by the Deutsche Forschungsgemeinschaft via the SFB 625 is acknowledged.

■ REFERENCES

- (1) Marx, D.; Hutter, J. *Ab Initio Molecular Dynamics: Basic Theory and Advanced Methods*; Cambridge University Press: Cambridge, UK, 2009.
- (2) MacKerell, A. D., Jr. *J. Comput. Chem.* **2004**, *25*, 1584–1604.
- (3) Frenkel, D.; Smit, B. *Understanding Molecular Simulation*; Academic Press: San Diego, CA, 2002.
- (4) Jorgensen, W. L.; Maxwell, D. S.; Tirado-Rives, J. *J. Am. Chem. Soc.* **1996**, *118*, 11225–11236.
- (5) Cornell, W. D.; Cieplak, P.; Bayly, C. I.; Gould, I. R.; Merz, K. M.; Ferguson, D. M.; Spellmeyer, D. C.; Fox, T.; Caldwell, J. W.; Kollman, P. A. *J. Am. Chem. Soc.* **1995**, *117*, 5179–5197.
- (6) Wang, J.; Wolf, R. M.; Caldwell, J. W.; Kollman, P. A.; Case, D. A. *J. Comput. Chem.* **2004**, *25*, 1157–1174.
- (7) Schuler, L. D.; Daura, X.; van Gunsteren, W. F. *J. Comput. Chem.* **2001**, *22*, 1205–1218.
- (8) Oostenbrink, C.; Villa, A.; Mark, A. E.; van Gunsteren, W. F. *J. Comput. Chem.* **2004**, *25*, 1656–1676.
- (9) Paton, R. S.; Goodman, J. M. *J. Chem. Inf. Model.* **2009**, *49*, 944–955.
- (10) Sheu, S.-Y.; Yang, D.-Y.; Selzle, H. L.; Schlag, E. W. *J. Phys. Chem. A* **2008**, *112*, 797–802.
- (11) Deng, N.-J.; Cieplak, P. *Biophys. J.* **2010**, *98*, 627–636.
- (12) Ricci, C. G.; de Andrade, A. S. C.; Mottin, M.; Netz, P. A. *J. Phys. Chem. B* **2010**, *114*, 9882–9893.
- (13) Freddolino, P. L.; Park, S.; Roux, B.; Schulten, K. *Biophys. J.* **2009**, *96*, 3772–3780.
- (14) Freddolino, P. L.; Harrison, C. B.; Liu, Y.; Schulten, K. *Nat. Phys.* **2010**, *6*, 751–758.
- (15) Yoda, T.; Sugita, Y.; Okamoto, Y. *Chem. Phys. Lett.* **2004**, *386*, 460–467.
- (16) Mu, Y.; Kosov, D. S.; Stock, G. *J. Phys. Chem. B* **2003**, *107*, 5064–5073.
- (17) Piana, S.; Lindorff-Larsen, K.; Shaw, D. E. *Biophys. J.* **2011**, *100*, L47–L49.
- (18) Evans, E. *Annu. Rev. Biophys. Biomol. Struct.* **2001**, *30*, 105–128.
- (19) de Graff, A. M. R.; Shannon, G.; Farrell, D. W.; Williams, P. M.; Thorpe, M. F. *Biophys. J.* **2011**, *101*, 736–744.
- (20) Gräter, F.; Grubmüller, H. *J. Struct. Biol.* **2007**, *157*, 557–569.
- (21) Allen, W. J.; Bevan, D. R. *Biochemistry* **2011**, *50*, 6441–6454.
- (22) Jorgensen, W. L.; Tirado-Rives, J. *J. Am. Chem. Soc.* **1988**, *110*, 1657–1666.
- (23) Wang, L.; Vyotsky, M. O.; Bogdan, A.; Bolte, M.; Böhmer, V. *Science* **2004**, *304*, 1312–1314.
- (24) Molokanova, O.; Podoprygorina, G.; Bolte, M.; Böhmer, V. *Tetrahedron* **2009**, *65*, 7220–7233.
- (25) Janke, M.; Rudzevich, Y.; Molokanova, O.; Metzroth, T.; Mey, I.; Diezemann, G.; Marszałek, P.; Gauss, J.; Böhmer, V.; Janshoff, A. *Nat. Nanotechnol.* **2009**, *4*, 225–229.
- (26) Schlesier, T.; Metzroth, T.; Jahnshoff, A.; Gauss, J.; Diezemann, G. *J. Phys. Chem. B* **2011**, *115*, 6445–6454.
- (27) Böhmer, V. *Angew. Chem., Int. Ed. Engl.* **1995**, *34*, 713–745.
- (28) Abraham, W. J. *Inclusion Phenom. Macrocyclic Chem.* **2002**, *43*, 159–174.
- (29) Ikeda, A.; Shinkai, S. *Chem. Rev.* **1997**, *97*, 1713–1734.
- (30) Zhang, G.-F.; Zhan, J.-Y.; Li, H.-B. *Org. Lett.* **2011**, *13*, 3392–3395.
- (31) Spruell, J. M.; Paxton, W. F.; Olsen, J.-O.; Benítez, D.; Tkatchouk, E.; Stern, C. L.; Trabolsi, A.; Friedman, D. C., III; W., A. G.; J. F. Stoddart, J. F. *J. Am. Chem. Soc.* **2009**, *131*, 11571–11580.
- (32) Hess, B.; Kutzner, C.; van der Spoel, D.; Lindahl, E. *J. Chem. Theory Comput.* **2008**, *4*, 435–447.
- (33) Schüttelkopf, A. W.; van Aalten, D. M. F. *Acta Crystallogr.* **2004**, *D60*, 1355–1363.
- (34) Cornell, W. D.; Cieplak, P.; Bayly, C. I.; Kollman, P. A. *J. Am. Chem. Soc.* **1993**, *115*, 9620–9631.
- (35) Anisimov, V. M.; Lamoureux, G.; Vorobyov, I. V.; Huang, N.; Roux, B.; MacKerell, A. D., Jr. *J. Chem. Theory Comput.* **2005**, *1*, 153–168.
- (36) Vanqualef, E.; Simon, S.; Marquant, G.; Garcia, E.; Klimerak, G.; Delepine, J. C.; Cieplak, P.; Dupradeau, F.-Y. *Nucleic Acids Res.* **2011**, *39*, 511–517.
- (37) Frisch, M. J. et al. *Gaussian 09, Revision A.1*; Gaussian, Inc.: Wallingford, CT, 2009.
- (38) Szabo, A.; N. S. Ostlund, N. S. *Modern Quantum Chemistry*; Dover: New York, 1996.
- (39) Hariharan, P. C.; Pople, J. A. *Theor. Chim. Acta* **1973**, *28*, 213–222.
- (40) Case, D. A. et al. *AMBER11*; University of California: San Francisco, 2010.
- (41) Darden, T.; York, D.; Pedersen, L. *J. Chem. Phys.* **1993**, *98*, 10089–10092.
- (42) Allen, M.; Tildesley, D. *Computer Simulations of Liquids*; Oxford Science Publications: Oxford, UK, 1987.
- (43) Hess, B.; Bekker, H.; Berendsen, H. J. C.; Fraaije, J. G. E. M. *J. Comput. Phys.* **1997**, *18*, 1463–1472.
- (44) Bussi, G.; Donadio, D.; Parrinello, M. *J. Chem. Phys.* **2007**, *126* (014101), 1–7.
- (45) Parrinello, M.; Rahman, A. *J. Appl. Phys.* **1981**, *52*, 7182–7190.
- (46) Aicart, E.; Junquera, E. *J. Chem. Eng. Data* **1995**, *40*, 1225–1227.
- (47) Rief, M.; Grubmüller, H. *Chem. Phys. Chem.* **2002**, *3*, 255–261.
- (48) Bell, G. *Science* **1978**, *200*, 618–627.
- (49) Seifert, U. *Europhys. Lett.* **2002**, *58*, 792–798.
- (50) Li, F.; Leckband, D. *J. Chem. Phys.* **2006**, *125*, 194702:1–9.
- (51) Diezemann, G.; Janshoff, A. *J. Chem. Phys.* **2008**, *129*, 084904:1–10.
- (52) Bornschlög, T.; Rief, M. *Phys. Rev. Lett.* **2006**, *96*, 118102:1–4.
- (53) Paci, E.; Ciccotti, G.; Ferrario, M. *Chem. Phys. Lett.* **1991**, *176*, 581–587.
- (54) Villa, A.; Peter, C.; van der Vegt, N. F. A. *J. Chem. Theory Comput.* **2010**, *6*, 2434–2444.
- (55) Erdmann, T.; Schwarz, U. S. *Europhys. Lett.* **2004**, *66*, 603–609.